Biophysical Reports

ARTICLE

Diffusion and interaction dynamics of the cytosolic peroxisomal import receptor PEX5

S. Galiani,[1,2,*] K. Reglinski,[1,3,4,5] P. Carravilla,[3,4,6,7] A. Barbotin,[1,8] I. Urbančič,[1,9] J. Ott,[10] J. Sehr,[10] E. Sezgin,[1,11] F. Schneider,[12] D. Waithe,[2,13] P. Hublitz,[15] W. Schliebs,[10] R. Erdmann,[10] and C. Eggeling[1,2,3,4,14,*]

[1]MRC Human Immunology Unit, MRC Weatherall Institute of Molecular Medicine, University of Oxford, Oxford, UK; [2]Wolfson Imaging Centre, MRC Weatherall Institute of Molecular Medicine, University of Oxford, Oxford, UK; [3]Leibniz-Institute of Photonic Technologies e.V., Jena, Germany; [4]Institute of Applied Optic and Biophysics, Friedrich-Schiller University Jena, Jena, Germany; [5]University Hospital Jena, Jena, Germany; [6]Department of Biochemistry and Molecular Biology, University of the Basque Country (UPV/EHU), Bilbao, Spain; [7]Instituto Biofisika (UPV/EHU, CSIC), University of the Basque Country, Leioa, Spain; [8]Department of Engineering Science, University of Oxford, Oxford, UK; [9]Laboratory of Biophysics, Condensed Matter Physics Department, Jožef Stefan Institute, Ljubljana, Slovenia; [10]Institute of Biochemistry and Pathobiochemistry, Systems Biochemistry, Ruhr-University Bochum, Bochum, Germany; [11]Science for Life Laboratory, Department of Women's and Children's Health, Karolinska Institutet, Solna, Sweden; [12]Kennedy Institute for Rheumatology, University of Oxford, Oxford, UK; [13]WIMM Centre for Computational Biology , MRC Weatherall Institute of Molecular Medicine, University of Oxford, Oxford, UK; [14]Jena Center for Soft Matter (JCSM), Jena, Germany; and [15]WIMM Genome Engineering Services, MRC Weatherall Institute of Molecular Medicine, University of Oxford, Oxford, UK

ABSTRACT Cellular functions rely on proper actions of organelles such as peroxisomes. These organelles rely on the import of proteins from the cytosol. The peroxisomal import receptor PEX5 takes up target proteins in the cytosol and transports them to the peroxisomal matrix. However, its cytosolic molecular interactions have so far not directly been disclosed. Here, we combined advanced optical microscopy and spectroscopy techniques such as fluorescence correlation spectroscopy and stimulated emission depletion microscopy with biochemical tools to present a detailed characterization of the cytosolic diffusion and interaction dynamics of PEX5. Among other features, we highlight a slow diffusion of PEX5, independent of aggregation or target binding, but associated with cytosolic interaction partners via its N-terminal domain. This sheds new light on the functionality of the receptor in the cytosol as well as highlighting the potential of using complementary microscopy tools to decipher molecular interactions in the cytosol by studying their diffusion dynamics.

WHY IT MATTERS The peroxisomal import receptor PEX5 transports newly synthesized proteins from the cytosol to the peroxisomal matrix. Here, the cytosolic diffusion and interaction dynamics of PEX5 are characterized by advanced microscopic spectroscopy methods, revealing a so far unknown interaction partner.

INTRODUCTION

Cellular signaling critically depends on accurate interaction between molecules, and alterations may lead to severe cellular dysfunctions. For example, organelle functions naturally rely on molecular interactions in the cellular cytosol, such as the import of proteins into peroxisomes. Peroxisomes are ubiquitous organelles in eukaryotic cells fulfilling many metabolic functions that are cell-type specific and variable as a response to environmental changes. Consequently, the pool of peroxisomal matrix proteins needs to be continuously adapted, entailing the necessity of a highly dynamic import system. Peroxisomal matrix proteins are synthesized on free ribosomes in the cytosol and transported into the organelle post-translationally. The peroxisomal cargo receptor PEX5 is one of the key proteins in the peroxisomal import process (Fig. 1).

Most peroxisomal matrix proteins imported by PEX5 contain a peroxisomal targeting signal type 1 (PTS1) at their C-terminus, while cargo proteins with the less abundant PTS2 targeting sequence are recognized and transported by the PTS2 receptor PEX7. PEX5 appears as two splice variants, a shorter one (PEX5S) that can only recognize PTS1 cargo proteins and a longer variant (PEX5L) that contains an additional PEX7 binding

Submitted February 9, 2022, and accepted for publication March 24, 2022.

*Correspondence: silvia.galiani@rdm.ox.ac.uk or christian.eggeling@uni-jena.de

S. Galiani and K. Reglinski contributed equally to this work.

Editor: Jörg Enderlein.

https://doi.org/10.1016/j.bpr.2022.100055

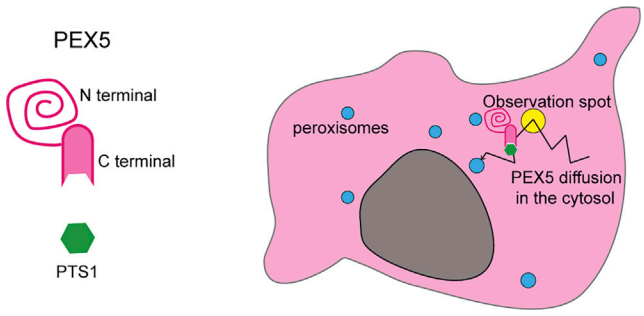

FIGURE 1 PEX5 receptor. Left: schematic of the PTS1 receptor PEX5 and its binding partner, a PTS1 cargo protein. PEX5 consists of a globular C-terminal domain, which binds the PTS1-containing peroxisomal matrix proteins, and an unstructured N-terminal domain, which is needed for peroxisomal docking, integration of PEX5 into the peroxisomal membrane, and translocation of the PTS1 cargo protein across the membrane. Right: schematic of a cell expressing full-length PEX5 (magenta) and eGFP-PTS1 (green when binding PEX5 and cyan at the peroxisomes). The diffusion (represented by the *black arrow*) of PEX5 and the PEX5/eGFP-PTS1 receptor/cargo complex is studied in the cytosol. Here the fluorescence fluctuations are measured in an observation spot (yellow).

site (1). Therefore, the import pathways of PTS1 and PTS2 proteins merge with the long splice form. After binding, PEX5 directs the cargo receptor complexes to the peroxisomal membrane and initiates the cargo translocation by interacting with the peroxisomal membrane protein PEX14. At the peroxisomal membrane, PEX5 is integrated into the membrane, forming a transient translocation pore to import the cargo protein into the peroxisome (2). Consequently, PEX5 is a shuttling receptor with a much larger fraction in the cytosol (searching to bind newly synthesized cargo proteins), and only a small fraction at a time binds to the peroxisomal membrane (mainly involved in cargo translocation) (3,4). While it has been shown that the import of cargo proteins depends on the affinity of the PTS1 signal sequence to PEX5 (5,6), no further details are known about the interaction time scales and, thus, dynamics, i.e., the diffusion dynamics of the cargo receptor complex in the cytosol are basically completely unknown, which yet can highlight important details of the involved interaction dynamics.

Therefore, it is essential to employ observation techniques that disclose details of interaction dynamics in the living cells with high accuracy. One remedy is to study molecular diffusion dynamics, since diffusion will be hampered upon interactions (7). Various fluorescence microscopy approaches have been employed and optimized to detail molecular diffusion dynamics especially in the cellular plasma membrane, such as fluorescence recovery after photobleaching (FRAP) (8), fluorescence correlation spectroscopy (FCS) (9–12), or single-particle tracking (SPT) (13,14), even in combination with super-resolution microscopy approaches (15,16). As a result of adding one spatial dimension from two- (2D) to three-dimensional (3D) diffusion, the application of the above techniques to cytosolic studies is more elaborate than on membranes and usually requires more data mining (10–12,17–20). Therefore, it is necessary to further adapt techniques for studying cytosolic interaction dynamics and also to combine them with dedicated complementary tools and controls.

Here, we present a detailed characterization of the diffusion and, thus, interaction dynamics of human cytosolic PEX5 in vitro and in living cells by combining state-of-the-art microscopy and spectroscopy techniques such as FCS in combination with multi-color detection and (super-resolution) stimulated emission depletion (STED) microscopy together with biological manipulation such as CRISPR/Cas9 and model systems. As a result, we demonstrated free diffusion of PEX5 in the cytosol, which was found to be unexpectedly slow and independent of cargo binding. Among many controls, we investigated PEX5 oligomerization, interactions with other proteins of the PTS2 import pathway, binding to constituents of the peroxisomal membrane, or association with the cytoskeleton, whereby we could show that none of these influence PEX5 diffusion. Interestingly, the slow diffusion of PEX5, which depended on its N-terminal half, was not linked to the intrinsically disordered structure of this region. By using the cell-derived giant plasma membrane vesicle (GPMV) model system and recombinant proteins in solution, we showed that the slow diffusion of PEX5 only occurred in the presence of cytosolic components, indicating that the characteristic diffusion of PEX5 is strictly linked to cytosolic factors yet to be identified.

MATERIALS AND METHODS

Plasmids

Sequences of the primers used are shown in Table S1.

For the simultaneous expression of different PEX5 variants together with eGFP-SKL (eGFP-PTS1), we used the dual-expression plasmid pIRES2/eGFP-SKL as described previously (21). First, a SNAP-tag was integrated by amplifying the SNAP sequence with plasmids RE4692/RE4693 and restriction sites *Sal*I/*Bam*HI. Thereafter, the full-length PEX5L was amplified from pIRES2 PEX5L/eGFP-SKL (22) with primers RE4640/RE4641 and cloned into the pIRES2 SNAP/eGFP-SKL using *Bgl*II/*Sal*I restriction sites. This pIRES2 PEX5L-SNAP/eGFP-SKL plasmid was used to construct all variations of PEX5L for the FCS measurements. Most of these variations were created using FastCloning (23). In brief, the vector backbone and the insert were amplified by PCR with overlapping ends. Thereafter, PCR products were mixed, the template DNA was digested with *Dpn*I, and overlapping sticky ends were annealed. Here the vector backbone was amplified from the pIRES2 PEX5L-SNAP/eGFP-SKL and the insert from different sources:

For PEX5-C-Term (pIRES2 PEX5L 1-335-SNAP/eGFP-SKL): vector amplification with primers RE4816/ RE4817, and insert amplification from pIRES2 PEX5L/eGFP-SKL with primers RE6194/RE6195.

For PEX5-N-Term (pIRES2 PEX5L 314-639-SNAP/eGFP-SKL), the PEX5L fragment was amplified with primers RE6196/RE6197 and subcloned into *Bgl*II/*Sal*I digested pIRES2 PES5L-SNAP/eGFP-SKL.

For PEX5 S600W-SNAPeGFP-SKL, the PEX5 S600W sequence was amplified with primers KR001/KR002 from PEX5 S600W (24) in pcDNA3.1 and ligated into the *Bgl*II/*Sal*I digested pIRES2 PEX5-SNAP/eGFP-SKL.

The PEX5S-HALO/eGFP-SKL plasmid was created from the pIRES2/eGFP-SKL as well. First, the HaloTag was integrated by amplification with primers RE4694/RE4695 and subcloning of the PCR product into the pIRES2/eGFP-SKL using restriction sites *Sal*I/*Bam*HI. Thereafter, the full-length PEX5S was amplified with primers RE4640/RE4641 and cloned into the pIRES2 HALO/eGFP-SKL using *Bgl*II/*Sal*I restriction sites.

For pIRES2 *Tb*Pex5 1-340 SNAP-eGFP-SKL: vector amplification with primers RE6496/RE6486; insert amplification from *Tb*PEX5 (25) with primers RE6490/RE6491.

The SNAP-eGFP fusion construct was created by amplifying the SNAP fragment from pIRES-PEX5-SNAP/eGFP-SKL with the primers KR011/KR012 and subcloning it into *Hin*dIII/*Bam*HI digested peGFP-N1 (Clontech, Mountain View, CA).

The PEX5L-SNAP fusion construct was created by amplifying the SNAP fragment from pIRES-PEX5-SNAP/eGFP-SKL with the primers KR022/KR026 and subcloning it into *Sal*I/*Not*I digested peGFP-N1 (Clontech).

For the heterologous expression of eGFP fusion proteins in *Escherichia coli*, the pET-9d (Merck, Darmstadt, Germany) vector was used. Here the N-terminal sequences of human PEX5L (amino acids (aa) 1–335) and PEX5 from *Trypanosoma brucei* (aa 1–340) were fused to eGFP using the FastCloning approach. The pET-9d His *Hs*PEX5(1–335) was amplified using the primers RE7008/RE7009, and eGFP was amplified with primers RE7010/ RE7011. This vector was then used to construct the pET-9d His *Tb*PEX5(1–340) eGFP by amplifying the backbone with the primers RE7012/RE7013 and the *Tb*PEX5(1–340) using the primers RE7016/RE7017.

Recombinant proteins

For measurement of diffusion coefficients of the N-terminal halves of *Hs*PEX5L (aa 1–335) and *Tb*PEX5 (aa 1–340), both fused to eGFP, these were heterologously expressed in *E. coli* and purified using Ni-NTA columns as described elsewhere (26). In brief, the cells were homogenized by sonication, sedimented, and the supernatant incubated with the Ni-NTA matrix for 1 h. Thereafter, the proteins were eluted with a 10–500 mM imidazole gradient. For confocal FCS measurements, concentrations of 5 nM for *Hs*PEX5L N-Term and 20 nM for *Tb*PEX5 N-Term were used. eGFP was obtained from Novus Biologicals (Littleton, CO) and used at a final concentration of 10 nM.

Subcellular fractionation to purify cytosol from human cells

Human HEK-293 cells were harvested from two T75 flasks for each experiment. The cells were incubated in 1 mL of digitonin buffer (150 mM NaCl, 50 mM HEPES, 25 μg/mL digitonin) for 10 min, as described in (27). After sedimentation of the remaining cell fragments (2000 × g, 4°C, 5 min), the cytosol was in the supernatant. For measurement of diffusion speed, the recombinant proteins were diluted with purified cytosol to 5 nM for His-*Hs*PEX5L(1–335) and 20 nM for His-*Tb*PEX5(1–340) and analyzed by point FCS.

Construction of HEK-293 PEX5 and PEX14 knockout cell lines using CRISPR/Cas9

Deletion of PEX5 and PEX14 in HEK-293 cells was accomplished using a dual single-guide RNA (sgRNA) approach. In particular, the sgRNA pairs targeted defined critical exons of PEX5 (exon 2) and PEX14 (exon 3), resulting in nonsense-mediated mRNA decay, the likely event after homozygous deletion in both cases. sgRNAs were selected using the CRISPOR algorithm (28). sgRNAs targeting the intron upstream of the respective splice branch point were cloned into pX458 (Addgene 48138, Dr. Feng Zhang), and sgRNAs targeting the intron downstream of the target exon were cloned into pX458-Ruby (Addgene 110164, Dr. Philip Hublitz). sgRNA ON-target efficiency was evaluated by Surveyor assay (Surveyor Mutation Detection Kit; IDT, Coralville, IA), and the following guides were chosen: PEX14 5′, GGatcagctcgaatggagatc; PEX14 3′, GGacccccagtgggg catgc; PEX5 5′, ggggtcgcagcaaaagcact; PEX5 3′, Ggtttataaacgctcag taag (capitalized nucleotides within the sgRNA sequences correspond to added G residues to allow for proper polymerase III transcription). Cells were transfected with both sgRNA expressing plasmids. Seventy-two hours post transfection, double mRuby2/eGFP-positive cells were sorted using fluorescence-activated cell sorting into 96-well plates. After expansion, cells were analyzed by genomic PCR using primers spanning the deleted region (PEX14 FW, cagcatacagggcacaagggcgg; PEX14 RV, tgctactgaatgctgcctttgcc; PEX5 FW, ggtccaggccccttttgtggaggc; PEX5 RV, aacaagcaggcattct cattcgg). Mutations were verified by Sanger sequencing of the subcloned amplicons, and absence of the respective protein was confirmed by immunoblotting. Of note, we obtained several clones in which the excised exon was found inverted and reinserted, nevertheless giving a full knockout (KO) phenotype as described (29). All clones selected for this study were confirmed homozygous deletions.

Sample preparation for live-cell FCS measurements

Human fibroblasts (GM5756-T (RRID:CVCL_VQ75)) (30), HEK 293 (ATCC, Manassas, VA), HEK KO PEX5, and HEK KO PEX14 cells were maintained in a culture medium consisting of Dulbecco's modified Eagle's medium with 4500 mg glucose/L, 110 mg sodium pyruvate/L supplemented with 10% fetal bovine serum, glutamine (2 mM), and penicillin-streptomycin (1%). The cells were cultured at 37°C/5% CO_2. Cells were grown on a #1.5 μ-Dish 35 mm (World Precision Instruments, Sarasota, FL) and transfected with 2.5 μg of DNA per dish using Lipofectamine 3000 transfection reagent (Invitrogen, Carlsbad, CA). Twenty-four hours after transfection, the cells were incubated at 37°C for 40 min with silicon rhodamine (SiRo) SNAP-tag (1.2 μM), SNAP-Cell 647-SiR, or SNAP-Cell 505-Star (both from New England Biolabs, Ipswich, MA) to label the SNAP-tagged PEX5L. HaLo-tagged PEX5S was labeled with Halo-Cell 647-SiR (New England Biolabs) in a final concentration of 1 μM. The samples were washed twice for 20 min with 1 mL of culture medium in an incubator at 37°C. For the measurement the culture medium was substituted with L-15 (Leibovitz's) medium (Thermo Fisher Scientific, Waltham, MA) and placed on the microscope for data acquisition for no longer than 1 h. Each sample was kept in culture medium in the incubator until the measurement started.

Confocal FCS measurements

Confocal live-cell FCS measurements

Confocal FCS measurements on living cells were performed at a confocal Zeiss (Oberkochen, Germany) LSM 880 microscope equipped for FCS. The microscope provides 488 nm and 633 nm excitation lines focused into the sample via a 40×/1.2 (Zeiss C-APOCHROMAT) water immersion objective lens. Excitation powers were set respectively for calibration solution and cytosolic measurements at 7 μW and 0.5 μW for the 488 nm excitation laser and at 6 μW and 1 μW for the 633 nm excitation laser (power measured at the objective

lens). The fluorescence emission was split into two detectors depending on the characteristic emission wavelengths and the counts per molecule maximized acting on the correction collar of the objective lens. A time trace was recorded for each spectral emission channel and both fluorescence auto- and cross-correlation curves calculated using Zen software (Zeiss).

To calibrate the illumination volume for both excitation lines, an 18 nM solution containing a 1:1 mix of Alexa Fluor 647 ($D = 330$ $\mu m^2/s$) (16) and Alexa Fluor 488 ($D = 430$ $\mu m^2/s$) (31) was used in a μ-slide 8-well dish (ibidi, Martinsried, Germany). The excitation beams were focused a few micrometers away from the glass of the microscope slides into the solution, and an FCS measurement was repeated three times with a duration of 5 s per time-trace recording. The characteristic confocal full width at half maximum, d, was calculated, knowing the diffusion coefficient, D, and deducing an average transit time, τ_D, from the three acquired FCS curves, related by Eq. 1:

$$d = \sqrt{8 \ln (2) \tau_D D}; \quad D = \frac{d^2}{8 \ln(2) \tau_D}. \tag{1}$$

The calibrated d per excitation line was then utilized to calculate D for each protein of interest labeled with a dye with similar spectral characteristics, implying the same excitation volume (eGFP and SiRo in our experiments). Each illumination volume was calibrated every day to monitor microscope performance and take small volume variations into consideration. Once the focal volume was calibrated, the actual measurements on live cells could be performed. Healthy cells expressing eGFP and/or SNAP/Halo-tagged SiRo signal were selected by visual inspection of the samples. In each sample, three data-collection locations in the cytosol of each cell were selected and the time-trace acquisition repeated three times per each set position for a 5 s recording. At least 10 cells for each sample were measured for the acquisition of one data set. Each data set was collected on at least three biological replicates. No appreciable photobleaching occurred during the acquisition.

The Zeiss Zen software provides already auto-correlated or cross-correlated curves that were analyzed via FoCuS-point software (32). The data were fit using a 3D diffusion model that includes a triplet component. The overall generic model for analyzing the correlation curves was

$$G_N(\tau) = O_f + G_0[G_D(\tau) G_T(\tau)], \tag{2}$$

where τ represents the correlation lag time, O_f represents the offset (fixed to 1), G_0 is the amplitude of the correlation function at $\tau = 0$, $G_D(\tau)$ is describing all correlation components relating to diffusion processes, and $G_T(\tau)$ is an optional term accounting for a triplet state (dark state kinetics).

To analyze our data, we used the following triplet equation:

$$G_T(\tau) = 1 + \left(\frac{T}{1-T}\right) e^{-(\tau/\tau_T)}, \tag{3}$$

where T is the average triplet amplitude and τ_T is the triplet correlation time that we fixed at 0.005 ms for SiRo and 0.04 ms for eGFP (33–35).

To analyze our cytosolic proteins' mobility ($G_D(\tau)$), we considered a 3D diffusion model with multiple component fitting possibility:

$$G_{3D}(\tau) = \sum_{k=1}^{D_S} A_k \left(1 + \left(\frac{\tau}{\tau_{xyk}}\right) \alpha^k\right)^{-1} \left(1 + \frac{\tau}{AR_k^2 \times \tau_{xyk}}\right)^{-1/2}, \tag{4}$$

where τ_{xyk} is the lateral diffusion rate coefficient and represents the time taken for the diffusing species Kth to move laterally through the illumination area with its fraction A_k. α is the anomalous factor, important for compensating for when the diffusion kinetics are non-ideal. The aspect ratio that describes the illumination volume AR was here fixed to 6 and α, the anomalous factor, fixed to 1.

The diffusion analysis was optimized by comparing the diffusion of PEX5L and PEX5 S600W, both expressed in combination with eGFP-PTS1 in human cells. Here, the dual plasmids PEX5L-SNAP/eGFP-PTS1 and PEX5L S600W-SNAP/eGFP-PTS1 were respectively expressed. When PEX5L S600W-SiRo was expressed in human fibroblasts, the collected correlation curves for this protein were fitted considering one diffusing component, as the S600W substitution inhibits PTS1 binding and therefore the PEX5 S600W cannot bind/co-diffuse with the eGFP-PTS1. Only a free component of its characteristic transit time and the corresponding diffusion coefficient have been considered and calculated.

To study the dynamics of PEX5L in cells expressing PEX5L-SNAP-SiRo, we initially introduced a two-component fitting model ($D_S = 2$ in the above model), trying to isolate a free diffusion contribution (that we could fix according to the previous analysis on PEX5L S600W) from a bound diffusion contribution (which we expected to diffuse together with PTS1 proteins). Clearly only one particular diffusion coefficient could be extracted from these data, comparable for PEX5L and PEX5 S600W, so the number of components that contribute to the fitting model related to PEX5L has been reduced to one. Since both variants of PEX5 (PTS1 binding competent PEX5L and the binding incompetent PEX5L S600W) are characterized by the same diffusion coefficient, this also indicated that the binding of eGFP-PTS1 to PEX5L-SNAP-SiRo did not influence the diffusion speed of the receptor.

When PEX5 S600W was expressed in combination with eGFP-PTS1, the collected curves for the cargo protein eGFP-PTS1 were fitted considering two distinct populations (eGFP-PTS1 can still bind to the endogenous PEX5, fully functional but not labeled). The bound component was fixed in our analysis in accordance with the PEX5L characteristic diffusion coefficient (recalculated accordingly for 488 nm illumination volume) and the PTS1 free diffusion component extracted from the acquired FCS curves as well as the proportion between bound and unbound fraction. The majority (more than 87% on average) of the PTS1 in these samples was found to be unbound.

In the case of eGFP-PTS1 expressed in combination with PEX5L (dual plasmid PEX5L-SNAP/eGFP-SKL), the fluorescence cross-correlation spectroscopy (FCCS) curves showed a clear co-diffusion of PEX5L and eGFP-PTS1 at a diffusion coefficient comparable with that of PEX5L. Therefore, we considered the calculated PEX5L diffusion coefficient as the bound contribution. We set this diffusion coefficient as the characteristic diffusion coefficient of eGFP-PTS1 when bound to PEX5L (recalculated accordingly for 488 nm illumination volume). Finally, we combined the extracted information obtained by eGFP-PTS1 bound diffusion and free diffusion coefficients (from PEX5 S600W/eGFP-SKL expression) to calculate the fraction of eGFP-PTS1 diffusing free and bound in the case of the simultaneous expression of PEX5L-SNAP/eGFP-SKL.

Each calculated correlation curve was inspected by eye and eventually discarded when showing features clearly outside of the expected fitting model. In most cases discarded measurements showed a bright spike in the time trace that biased the correlation curve, possibly caused by a fluorescent cluster or a whole peroxisome moving into the focal volume. We did not explore the PEX5L diffusion at the peroxisomal membrane, as there the protein mobility is slower than the photobleaching rate at the set conditions, which made it impossible to measure characteristic diffusion coefficients in this location.

Proteins in solution

FCS measurements were performed with a confocal PicoQuant (Berlin, Germany) MicroTime 200 machine and a Zeiss 880 laser scanning microscope. The microscopes provided 488 nm excitation lines focused into the sample via a 60×/1.2 (Olympus (Tokyo, Japan) UPlanSApo) and a 40×/1.2 (Zeiss C-APOCHROMAT) water immersion objective lenses, respectively. Excitation power was set to 5 μW to minimize eGFP photobleaching. Counts per molecule were maximized acting on the correction collar of the objective lenses. Time traces were recorded and FCS curves calculated for each measurement.

To measure the diffusion of eGFP and N-terminal part of PEX5L (human and from *T. brucei*, fused to eGFP) in solution, the proteins were diluted to ca. 10 nM. For each condition, recordings at three different spots were performed by measuring for 15–20 s five times at about 10 μm depth from the coverslip. Time traces acquired at the MicroTime were correlated using FoCuS-point software. Zeiss data were correlated using Zen software. The data were fitted using a 3D diffusion equation that includes a triplet component as described in the previous section.

AO-zSTED-FCS measurements

We used a custom STED microscope built around a RESOLFT microscope from Abberior Instruments (Göttingen, Germany) as described previously (4,36). The microscope was equipped with a 640 nm pulsed excitation laser focused into the sample via a 100×/1.4 (Olympus UPLSAPO) oil immersion objective lens. Excitation power was set to 6 μW (measured at the back aperture of the objective lens) in cells. A 755 nm depletion beam pulsed at 80 MHz (Spectra-Physics (Milpitas, CA) MaiTai, pulse-stretched by a 40 cm glass rod and a 100 m single-mode fiber) was modulated in phase using a spatial light modulator (SLM) (Hamamatsu (Hamamatsu, Japan) LCOSX10468-02). STED power was set to 16 mW for the aberration correction procedure and varied between 6 and 33 mW for STED-FCS measurements. The fluorescence emitted by the sample was collected back by the objective lens, filtered via emission filters and a pinhole, and detected using an avalanche photodiode (Hamamatsu). The system was equipped with a correlation card (Flex02-08D) to acquire both time traces and FCS curves. The microscope was controlled by Imspector software (Abberior Instruments). The SLM was employed for both phase-mask generation and aberration correction and controlled by a bespoke Python software as described in (36). z-STED illumination volume calibration was carried out on a bead sample, FluoSpheres (Thermo Fisher), crimson (625/645), diameter = 0.04 μm.

On each studied sample, an aberration correction procedure was run at the beginning of any data acquisition on one selected cell at approximately 3 μm from the slide into the cytosol. Data set collection consisted of a series of time traces acquired at increasing STED power distributed over a z-STED beam. For each sample at least five cells were selected and a STED power series (0, 7, 16, and 33 mW) was run over a selected point in the cytosol. Each measurement was acquired for 10 s and repeated three times. Each data set was collected on at least three biological replicates. The data were fitted using a standard 3D diffusion equation reported above (Eq. 4), with an α parameter set to 0.75 to account for a non-Gaussian point spread function in STED modality. (36,37). To account for the simultaneous decrease in lateral and axial size of the observation volume, we fitted STED-FCS curves using the model we previously developed (36). In short, confocal FCS curves were fitted first with an aspect ratio set to 4 (different from above as a higher-NA objective was used here). For z-STED recordings, the relative decreases in aspect ratios and lateral transit times with respect to the confocal values were fitted together using a single parameter, from which the axial transit times (t_z) were calculated. The relationship between lateral and axial dimension of the observation volume was calibrated using images of fluorescent beads, as described in (36). No appreciable photobleaching occurred during the acquisition.

RESULTS

Wild-type (PEX5L-SNAP) but not PTS1 non-binding mutant (PEX5L S600W-SNAP) shows co-diffusion with PTS1

To investigate the mobility of human PTS1 receptors and peroxisomal proteins in the cytosol, we expressed them in fusion with fluorescent proteins or with a SNAP-tag, which allows covalent binding of a fluorescent dye, in human fibroblasts (GM5756-T), and measured their diffusion and interaction characteristics by FCS and two-color FCCS under a confocal microscope. FCS provides information on the molecular diffusion by recording the fluorescence signal over time and analyzing the fluctuations caused by stochastic movement of fluorescent molecules in and out of the confocal observation volume. From the auto-correlation function (ACF) of these fluctuations, it is possible to extract the average transit time of a protein of interest through the observation volume and to determine its characteristic diffusion coefficient *D* and, thus, mobility as well as changes due to potential molecular interaction dynamics (10–12). In FCCS, the cross-correlation function (CCF) of the characteristic fluctuations of two differently labeled proteins is determined, highlighting their co-diffusion in addition to the mobility (Fig. 2 *a*) (38).

Specifically, we fluorescently labeled PEX5 with a SNAP-tag (denoted PEX5-SNAP) and the SNAP-tag binding dye SiRo (altogether denoted PEX5-SiRo). An artificial cargo protein was created by the conjugation of the tripeptide SKL, a peroxisomal targeting signal type 1, to the C-terminus of the enhanced green fluorescent protein (denoted eGFP-PTS1). We employed a dual-expression plasmid to ensure co-expression of both in the same cell (Fig. 2 *b*). We started with the longer variant of PEX5, PEX5L-SNAP, and in addition used the point mutant PEX5L S600W-SNAP (or PEX5L S600W-SiRo) as a control, which is not able to interact efficiently with PTS1 cargo proteins such as eGFP-PTS1 (24,39).

Using confocal microscopy imaging of eGFP-PTS1, we first compared the import efficiency after expressing PEX5L and PEX5L S600W in human fibroblasts, respectively (Fig. 2 *b*). Clearly, the wild-type (WT) protein showed strong import of eGFP-PTS1 into peroxisomes, as indicated by the higher abundance of fluorescence in the peroxisomes and reduced cytosolic fluorescence background, while cells transfected with

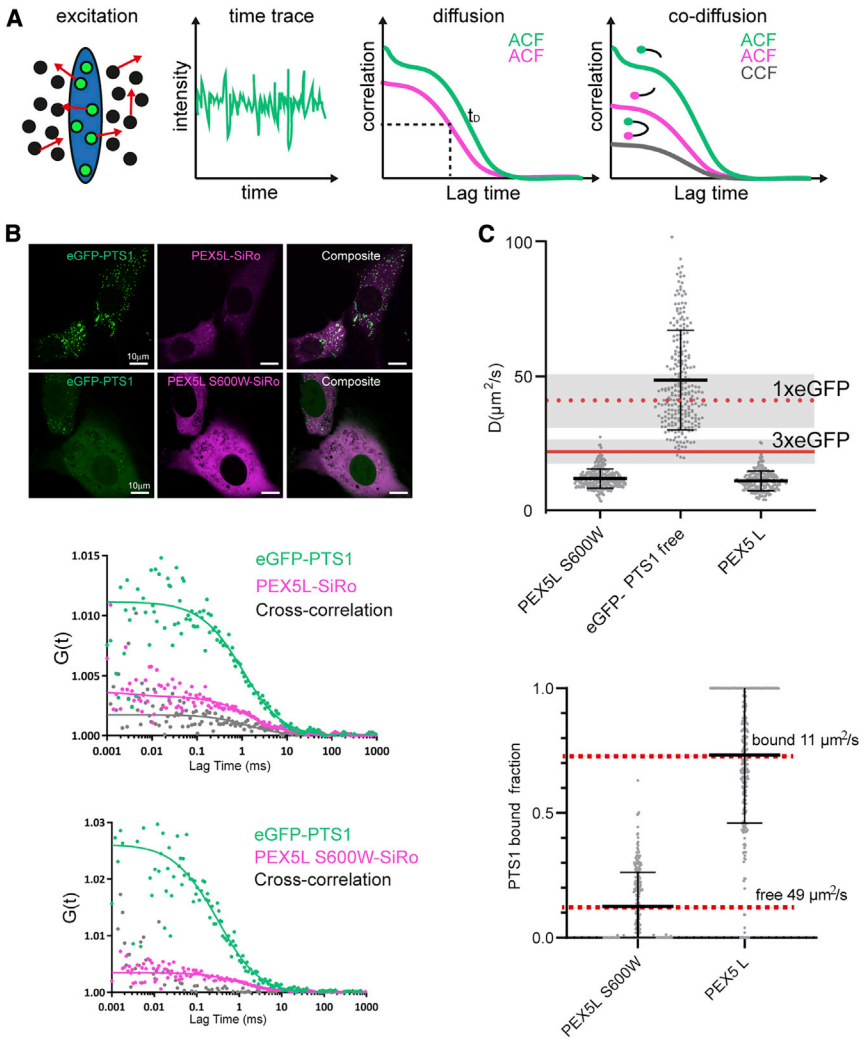

FIGURE 2 Characterization of the cell-cytosolic diffusion of PEX5L and eGFP-PTS1 by FCS. (*a*) Principle of FCS and FCCS. FCS provides the average transit time, τ_D, of diffusing fluorescent molecules (green) through the microscope's observation volume (blue) via calculation of the ACF from the time trace of the fluorescence signal. FCCS measures the interaction between two different species of molecules diffusing through the observation volume by calculation of the cross-correlation function between the two time traces. (*b*) Top: representative images of human fibroblast cells expressing eGFP-PTS1 (green) and PEX5L-SNAP-SiRo (magenta) (*upper*) and PEX5L S600W (*lower*) 24 h after transfection. Bottom: graphs showing the correlation curves $G(\tau)$ (*dots*) and fits of Eq. 3 to the data (*solid lines*) of each individual species (eGFP-PTS1, two components fit, PEX5L and PEX5L S600W) and their cross-correlation. Only PEX5L and eGFP-PTS1 signals cross-correlate (*gray curve*). (*c*) Top: diffusion coefficients (D) calculated from the fit of Eq. 3 to the auto-correlation curves with only one diffusing population for free PEX5L S600W ($D = 12 \pm 3.5$ $\mu m^2/s$), and a mainly free eGFP-PTS1 component ($D = 49 \pm 19$ $\mu m^2/s$). In cells expressing PEX5L only one slow-diffusing population was found for PEX5L ($D = 11 \pm 4$ $\mu m^2/s$), diffusing at the same speed as PEX5L S600W, independent of PTS1 cargo protein interaction. Bottom: fractions of eGFP-PTS1 diffusing together with PEX5L. eGFP-PTS1 was co-expressed with PEX5L S600W or PEX5L. In the case of PEX5L S600W, most of the eGFP-PTS1 diffused freely and only 12% of eGFP-PTS1 was bound to the endogenous PEX5. When PEX5L was expressed together with eGFP-PTS1, two diffusing populations (one bound to PEX5L and another free) for eGFP-PTS1 were found ($D = 11 \pm 4$ $\mu m^2/s$ and 49 ± 19 $\mu m^2/s$, respectively). In this case, around 25% of the eGFP-PTS1 diffused freely while around 75% co-diffused with PEX5L. Each dot in the graphs represents an individual FCS measurement (refer to "confocal live-cell FCS measurements" in materials and methods). The bars represent the mean and standard deviation. The mean values of the diffusion coefficients of freely diffusing eGFP (*dashed red line*) and 3xeGFP (fusion protein composed of three eGFP molecules, *solid red line*) expressed in the same cell line are displayed for comparison with eGFP-PTS1 and PEX5L, respectively.

PEX5L S600W were characterized by mainly cytosolic fluorescence background. Thus, in the latter case the import was less efficient, which was to be expected since only the pool of endogenous unlabeled PEX5 could transport and thus import eGFP-PTS1.

Fig. 2 *b* also highlights representative FCS (or ACF) and FCCS (or CCF) curves of cytosolic PEX5L-SiRo, PEX5L S600W-SiRo, and the co-expressed eGFP-PTS1. While the presence of non-zero and decaying ACFs of all proteins highlights their mobility, the CCFs differ between PEX5L-SiRo and PEX5L S600W-SiRo: the non-zero and decaying CCF of PEX5L-SiRo and eGFP-PTS1 disclose their co-diffusion and, thus, efficient binding, and the non-existing CCF in the case of PEX5L S600W-SiRo and eGFP-PTS1 reveals their expected missing interaction.

It is important to mention that we were only able to characterize mobility of the PEX5 proteins in the cytosol but not at the peroxisomal membrane, as the diffusion of PEX at peroxisomal membranes was so slow that photobleaching became a limiting factor (see materials and methods). However, we checked all cytosolic FCS and FCCS data for absence of bias due to photobleaching, as highlighted by constant (and not decreasing) average transit times through the observation volume within the employed excitation laser intensity range (40). Furthermore, we used FCCS to only qualitatively indicate the existence of co-diffusion between different potential binding partners but not to determine exact values of binding degrees. The latter would on one hand require detailed control experiments, such as quantification of green-red confocal

overlap (11,38), and on the other hand would in our case be biased by the presence of non-labeled endogenous proteins.

Detailed FCS analysis: Bound and unbound pools of cargo protein PTS1 and slow diffusion of PEX5 independent of PTS1 binding

We next analyzed the FCS data in more detail by fitting Eq. 1 to the ACF curves and extracting values of the diffusion coefficient D. The ACF curves of PEX5L-SiRo were well described by a one-component fit, revealing a rather slow mobility with a diffusion coefficient of $D = 11 \pm 3.5\ \mu m^2/s$. In contrast, we needed to include two populations with different mobility to accurately describe the ACF curves of the eGFP-PTS1 cargo. Instead of letting all parameters freely float (which led to rather inaccurate results), we rather extracted the diffusion coefficients of the two populations by assigning the slower component to eGFP-PTS1 bound to PEX5L-SiRo with the value of the transit time fixed to the corresponding value of $D = 11\ \mu m^2/s$ of PEX5L-SiRo, and the faster component to unbound eGFP-PTS1 with free-floating values of the transit time, resulting in $D = 49 \pm 19\ \mu m^2/s$ (see materials and methods for details) (Fig. 2 *c*). The distribution of values of D as highlighted in Fig. 2 *c* entail a Lorenz-like frequency distribution, as expected for free diffusion (41), and is not due to photobleaching (which we excluded from control experiments at different excitation intensities, see comment above) or other binding events. On average, around 75% of the eGFP-PTS1 was diffusion bound to the receptor (Fig. 2 *c*). However, the fractions of unbound and bound cargo protein varied between independent experiments, probably due to differences in the expression levels. We must also note that this fraction includes binding to expressed labeled as well as endogenous unlabeled PEX5. In general, all these factors impede the determination of exact absolute values of binding degrees (whether from FCS or FCCS data) or diffusion coefficients. However, we were rather interested in a qualitative assessment of binding by comparing relative values between different conditions, for which our approach seems appropriate.

Within the error bars, the diffusion coefficient of unbound eGFP-PTS1 ($D = 49 \pm 19\ \mu m^2/s$) was similar to that of cytosolic eGFP ($D = 41 \pm 11.5\ \mu m^2/s$), which is also of similar molecular weight (MW) (26.95 kDa (eGFP) against 27.4 kDa (eGFP-PTS1), Fig. S2) and non-interacting, highlighting free diffusion of unbound eGFP-PTS1 (Fig. 2 *c*). Still, these results proved that cargo proteins could be found both bound and unbound to its receptor. As a control, we also studied cells co-expressing the PEX5L S600W mutant and eGFP-PTS1. For PEX5L S600W-SiRo, we found $D = 12 \pm 3.5\ \mu m^2/s$, which is, within the errors, in the same range as PEX5L-SiRo ($D = 11 \pm 3.5\ \mu m^2/s$) and indicates that the mobility of PEX5L was independent of whether PTS1 is bound (PEX5L-SiRo) or not (PEX5L S600W-SiRo). Furthermore, we again could fit the FCS data of eGFP-PTS1 with two components, the unbound free form (with a transit time corresponding to $D = 49\ \mu m^2/s$, as before) and a form bound to PEX5L with the transit time fixed to a value corresponding to $D = 11\ \mu m^2/s$ of the mobility of PEX5L. However, the latter fraction was much lower (on average 12%) than for the previous WT PEX5L-SiRo expressing cells (on average 75%), since now only the small number of endogenous fully functional PEX5 was available to bind eGFP-PTS1 (Fig. 2 *c*).

In both WT PEX5L-SiRo and PEX5L S600W-SiRo expressing cells, the respective FCS data were both well described by a single diffusing population ($D = 11 \pm 3.5\ \mu m^2/s$ for PEX5L-SiRo and $D = 12 \pm 3.5\ \mu m^2/s$ for PEX5L S600W-SiRo). This finding was somewhat surprising, as two populations might have been expected, one fast component without and one slower one carrying PTS1 cargo proteins. However, as highlighted already in the previous paragraph, the mobility of PEX5L seemed to be independent of whether PTS1 was bound or not. To further detail this, we compared the mobility of PEX5L-SiRo and PEX5L S600W-SiRo against the similar weighed aggregate of three eGFP molecules (80.85 kDa for 3xeGFP compared with 91.39 kDa for PEX5L-SNAP, Fig. S2). 3xeGFP showed a diffusion coefficient about twice as high ($22 \pm 5\ \mu m^2/s$) as that for PEX5L, i.e., double the mobility (Fig. 2 *c*). Also, we confirmed the general slow and PTS1-independent diffusion of PEX5L for other cargoes such as eGFP-catalase and eGFP-SCP2. In all cases, diffusion of PEX5L-SiRo was equally slow (Fig. 3 *a*).

Consequently, the slowdown in diffusion of PEX5L is not due to its MW and is independent of PTS1 cargo binding.

The PTS2 pathway has no influence on PEX5 diffusion

As already highlighted, the PEX5 protein exists in two different isoforms, a long PEX5L and a short PEX5S form. While both isoforms interact with PTS1 cargo proteins, the long isoform PEX5L also contains a binding site for the PTS2 receptor PEX7. Thus, cargo-loaded PEX7 binds to PEX5L and bridges the binding of PTS2 cargo proteins to the PTS1 import receptor PEX5. To investigate any influence of the binding of PEX7/PTS2 complexes on the mobility of PEX5, we compared the diffusion of the PEX5L and PEX5S isoforms. Both variants were again jointly expressed in human fibroblasts (GM5756-T) from dual PEX5L-SNAP/eGFP-PTS1 and

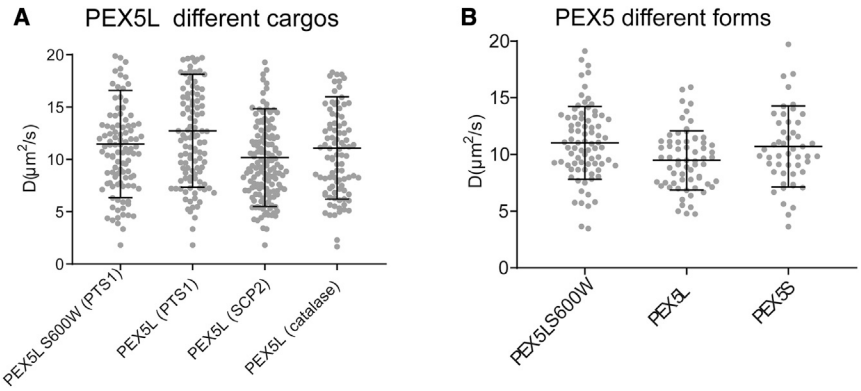

FIGURE 3 The diffusion of PEX5 is not influenced by binding cargo proteins or the PTS2 pathway: Diffusion coefficients of PEX5 in the cytosol of human fibroblasts from FCS measurements for different conditions. (*a*) The diffusion coefficient of PEX5L is independent of its cargo protein. Diffusion coefficients of PEX5L following transfection with the dual plasmids PEX5L S600W/eGFP-PTS1 and PEX5L/eGFP-PTS1 or with two plasmids, one encoding PEX5L-SNAP and the other eGFP-SCP2 or eGFP-Catalase, as labeled. (*b*) Diffusion of PEX5L and PEX5S is similar, i.e., independent of PTS2 import pathway. Diffusion coefficients of PEX5L S600W, PEX5 long isoform (PEX5L), and PEX5 short isoform (PEX5S). PEX5L has an additional binding site for the PTS2 receptor protein PEX7, which is lacking in PEX5S. Each dot in the graphs represents an individual FCS measurement (refer to "confocal live-cell FCS measurements" in materials and methods). Bars represent the mean and standard deviation.

PEX5S-Halo/eGFP-PTS1 plasmids, respectively, and fluorescent labeling realized with SiRo-SNAP and SiRo-Halo, respectively. Again, both variants showed undistinguishable mobility (Fig. 3 *b*), and we concluded that binding of PEX7 and its cargo was not rate limiting for the cytosolic mobility of PEX5.

Spot-variation FCS: PEX5L diffuses freely

As PEX5L showed an unexpectedly slow diffusion in the cytosol, we wanted to explore any heterogeneity in mobility (e.g., due to transient interactions) by comparing its diffusion mode with an inert and non-interacting and, thus, freely diffusing molecule (GFP-SNAP). For this, we employed spot-variation FCS (svFCS) (42). In svFCS, FCS data are taken for different sizes (or diameters) of the observation volume, and the dependency of the average transit time through the observation volume on the volume size is determined to highlight possible non-Brownian diffusion modes such as due to transient molecular interactions (16,42). Specifically, the plot of transit time against observation spot size (e.g., equatorial area) should be linear, with a *y* axis intercept of zero for Brownian and non-interacting diffusion and deviating otherwise.

Here, we realized svFCS by taking FCS data on a super-resolution STED microscope (STED-FCS) (16,43). STED-FCS allows measurements of the mobility of a fluorescent molecule for different sizes of the observation volume from around 200–250 nm and 700 nm in lateral and axial diameter to below 50–80 nm and 300 nm, respectively, by varying the intensity of the STED laser, which is added for the spatial confinement of the fluorescence emission (43). Using STED-FCS in the context of svFCS, free and hindered diffusion modes such as due to transient, interaction-evoked slowdowns could indeed be distinguishing and characterized (16,43). While STED-FCS is an established technique for the study of diffusion dynamics in two dimensions such as on membranes (44), our application at a 3D cytosolic level with required refined technical implementation (43,45–47). To tune the size of the effective fluorescence observation spot along the axial *z* direction, a top-hat intensity-shaped STED laser beam was overlapped with the standard excitation beam, whereby the performance was optimized by reducing possible optical aberrations using adaptive optics (AO) (36). In these AO-z-STED-FCS measurements, the STED laser power was increased stepwise to record FCS data and thus determine cytosolic PEX5L mobility at varying observation volumes (Fig. 4 *a*).

We first characterized the axial confinement of our observation volume from a standard confocal volume to the maximum compressed volume by acquiring a series of images of 40 nm sized fluorescent beads at different STED laser powers, highlighting a reduction of the axial diameter from 671 nm down to 256 nm (Fig. 4 *b*). We then used AO z-STED-FCS to measure the diffusion of eGFP-SNAP (labeled with SiRo dye) in the cytosol of living cells. eGFP-SNAP is an artificial protein that does not (to our knowledge) interacting with any cellular component and is therefore a suitable control to represent free diffusing modality. Its transit times through the observation volume decreased in coincidence with increasing STED power and, thus, confinement with a *y* axis intercept of zero (Fig. 4 *c*), indicating the absence of hindered diffusion (45). Using AO z-STED-FCS, we also highlighted free diffusion for cytosolic PEX5L and PEX5L S600W (labeled with SiRo). For both PEX5L and PEX5L S600W, the decrease in transit time with confinement of observation volume followed the same pattern as for freely diffusing eGFP-SNAP fusion protein (Fig. 4 *c*). Consequently, the slowed diffusion of PEX5L in the cytosol was not due to transient interactions with other more immobilized binding partners but rather a stable interaction with a permanent binding partner. Notably, this interaction was independent of the ability of PEX5 to bind to cargo proteins (as highlighted for non-PTS1-binding PEX5L S600W).

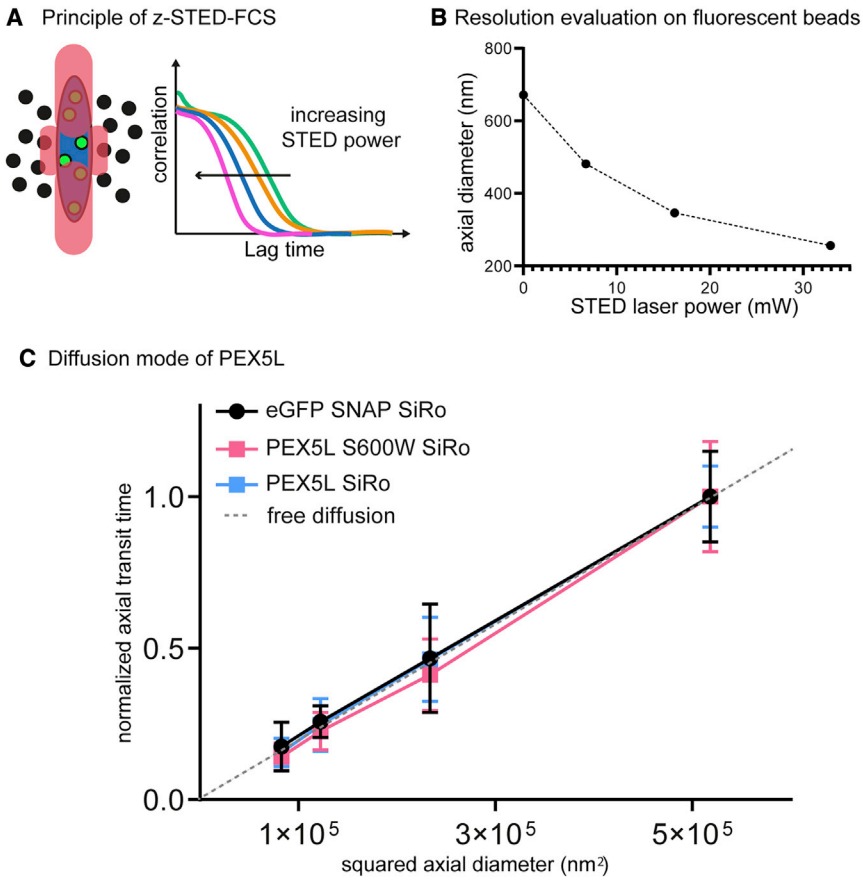

FIGURE 4 svFCS/AO-z-STED-FCS studies: PEX5L diffuses freely. (*a*) Principle of svFCS via AO-z-STED-FCS. The apparent diffusion coefficient is determined from FCS measurements at different observation spot sizes, as tuned by the intensity of the top-hat-shaped STED laser focus. The effective size of the observation spot (blue) decreases by increasing the power of the STED laser (red, left), which shortens the decay time of the ACFs (right). By analyzing the transit times in dependence of the axial equatorial observation area, mobility information at the sub-diffraction level can be extracted. (*b*) Calibration of the size of the axial equatorial observation area: 40 nm crimson beads were imaged at different STED laser powers (0 mW, 7 mW, 16 mW, 33 mW measured at the back aperture of the objective lens, top-hat-shaped laser focus), and the axial diameter (full width at half maximum) of the effective observation volume was evaluated from the images. (*c*) svFCS measurements of PEX5L diffusion. PEX5L, PEX5L S600W, and the eGFP-SNAP fusion protein used as control for free diffusion (all labeled with SiRo) were expressed in human fibroblasts, and their average axial transit time through the tuned observation volume was determined using svFCS via AO-z-STED-FCS. The relative decrease in axial transit times was normalized to the confocal case and plotted against the square of the axial diameter, all indicating free diffusion as highlighted by a straight line with zero intercept (*green dotted line*). Each dot in the graph represents the mean value of at least 30 measurements at each STED power (refer to "AO-zSTED-FCS measurements" in materials and methods). Bars represent the mean and standard deviation.

PEX5L does not form homo-oligomers within the cytosol

As highlighted, PEX5L integrates into the peroxisomal membrane to guide cargo proteins into the peroxisomal matrix. Owing to its accumulation at the membrane, it was previously hypothesized that PEX5L might oligomerize at the membrane or even already in the cytosol (48). To qualitatively investigate whether the observed slow cytosolic diffusion of PEX5L was linked to a possible homo-oligomerization, we conducted an FCCS study between differently labeled PEX5L to highlight their possible co-diffusion and thus potential homo-oligomerization. In Fig. 2 we show that our FC(C)S setup can indeed qualitatively pick up co-diffusion (i.e., oligomerization) events and distinguish them from non-interacting species through a non-zero versus zero amplitude of the cross-correlation curves.

Here, cells expressing PEX5L-SNAP were incubated with a solution containing an approximately 1:1 (mol/mol) mixture of the red-fluorescing SNAP-SiRo and green-fluorescing SNAP-Cell505 dyes. While the autocorrelation curves for each signal (SiRo and Cell505) were quite similar (Fig. 5 *b*) and confirmed the slow diffusion ($D = 10.5 \pm 4.5\ \mu m^2/s$ and $13 \pm 4\ \mu m^2/s$ for SiRo and Cell505 labeled PEX5L, respectively), as expected for the similarly tagged PEX5L proteins, there was no evidence of any cross-correlation signal. While we cannot exclude a weak or very transient interaction, we did not find any evidence of a strong PEX5L homo-oligomerization, i.e., a non-zero cross-correlation amplitude. In addition, the cytosolic mobility of PEX5L also did not change in a CRISPR/Cas9-derived PEX5 KO cell line (Fig. S1), precluding oligomerization of PEX5L with endogenous unlabeled PEX5.

As for the experiments of Fig. 2, we used FCCS here only to qualitatively test for co-diffusion and oligomerization. A more quantitative assessment would have required accurate control experiments and more reliable equal labeling degrees by red SiRo and green Cell505 dyes, which we, however, did not achieve for our cell systems.

Peroxisomal membranes and the cytoskeleton have no influence on the diffusion of PEX5L

PEX5L interacts with peroxisomal membrane proteins and integrates into the membrane during cargo translocation. Such interaction with the peroxisomal membrane

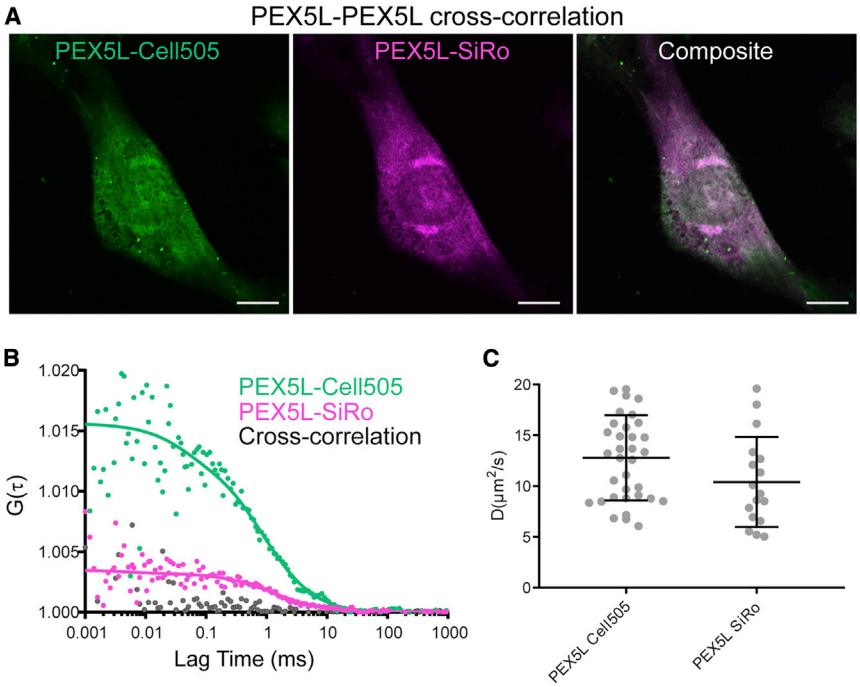

FIGURE 5 PEX5L does not form homo-oligomers in the cytosol, as highlighted on PEX5L-SNAP in the cytosol of human fibroblasts, co-labeled with SNAP-Cell505 and SNAP-SiRo dyes. (*a*) Representative confocal images, indicating localization in the cytosol for both labels. Scale bars, 10 μm. (*b*): Representative auto- and cross-correlation curves, highlighting no significant cross-correlation, i.e., co-diffusion of PEX5L-SNAP with itself. (*c*) Diffusion coefficients of PEX5L-SNAP-Cell505 and PEX5L-SNAP-SiRo from the respective auto-correlation data, indicating the same mobility for both. Each dot in the graph represents an individual FCS measurement. Bars represent the mean and standard deviation.

or membrane proteins could be a cause of the observed slowdown. Also, there are indications that PEX5L interacts with other organelles such as lipid droplets (49). Here, two different approaches were taken to test whether an interaction with peroxisomal membranes or other organelles could explain the slow PEX5L diffusion.

First, a cell-free model system in the form of GPMVs was used. Here, upon treatment of the cells with *N*-ethylmaleimide (NEM), the plasma membrane becomes detached from the cytoskeleton and forms free-standing vesicles that contain cytosolic proteins and are devoid of organelles and cytoskeleton (including microtubules and actin filaments) (Fig. 6 *a*) (50,51). Therefore, proteins in these vesicles cannot interact with the cytoskeleton or intracellular membranes. To compare the diffusion of PEX5L in cells and in GPMVs, we expressed PEX5L-eGFP (MW 99.3 kDa) and 3xeGFP (MW 80.85 kDa) in cells, generated GPMVs by treatment with NEM, and determined the diffusion coefficient of PEX5L-eGFP and 3xeGFP in both systems using FCS as before: $D = 10.5 \pm 2.5$ $\mu m^2/s$ (cells) and 20 ± 11 $\mu m^2/s$ (GPMVs) for PEX5L-eGFP, and $D = 25 \pm 4$ $\mu m^2/s$ (cells) and 39 ± 13.5 $\mu m^2/s$ (GPMVs) for 3xeGFP (Fig. 6 *b*).

For both PEX5L-eGFP and 3xeGFP there was a general increase in mobility in GPMVs compared with cells (factor 1.9 for PEX5L and 1.6 for 3xeGFP), owing to the decreased cytosolic crowding in GPMVs (50,51). Most importantly, the difference in mobility, or ratio between diffusion coefficients *D*, was similar in cells and GPMVs (D(3xeGFP)/D(PEX5L-eGFP) = 2.4 in cells compared with 2.0 in GPMVs), highlighting a slowdown of cytosolic PEX5L independent of potential interactions with organellar membranes or the cytoskeleton.

In a second approach, we investigated a potential interaction of PEX5L with peroxisomal membranes by determination of PEX5L mobility in a PEX14-deficient KO cell line. As PEX5L binds PEX14 at the peroxisomal membrane (52), the interaction of PEX5L with peroxisomal membranes should be inhibited in the absence of PEX14 or at least significantly decreased. Here, the dual plasmid expressing PEX5L and eGFP-PTS1 was expressed in a HEK 293 PEX14 KO cell line created by CRISPR/Cas9. In these cells, the diffusion coefficient of PEX5L ($D = 14 \pm 5$ $\mu m^2/s$) was, however, comparable with that in WT fibroblasts (16 ± 6 $\mu m^2/s$) or WT HEK cells (14.5 ± 4.5 $\mu m^2/s$), indicating that the interaction of PEX5L with PEX14 did not cause its cytosolic slowdown (Fig. 6 *c*).

Diffusion of PEX5L N- and C-terminal halves

PEX5L can be divided into two different functional parts, the structurally disordered N-terminal half (aa 1–335) (53,54), containing several WxxxxF/Y motifs that play a role in docking to the peroxisomal membrane (21,55), and the globular C-terminal half (aa 314–639) containing tetratricopeptide repeat (TPR) motifs, which interact with the PTS1 signal sequence (56) (schematics in Figs. 1 and 7 *a*, top).

We created truncations of PEX5 that comprise either the N-terminal or the C-terminal half of PEX5L (referred

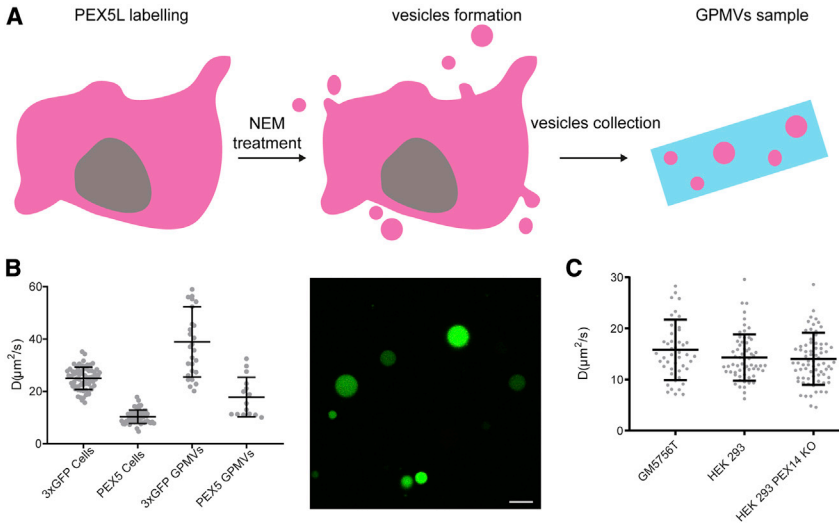

FIGURE 6 PEX5L is not slowed by peroxisomal membranes or cytoskeleton: measurements in cell-derived GPMVs. (*a*) Principle of GPMV formation. Cells expressing the labeled proteins of interest were incubated with NEM, which disrupts the interaction between the cortical actin and the plasma membrane, inducing the formation of blebs of the plasma membrane. These blebs contain cytosolic proteins but no organelles or a filamentous cytoskeleton. After blebbing of the cells the GPMVs can be collected and imaged. (*b*) Diffusion coefficient measured in intact cells and GPMVs. Human fibroblasts were transfected either with 3xeGFP, which has a MW of 81 kDa, close to that of PEX5L-eGFP (99.3 kDa), or PEX5L-eGFP itself. Using FCS, the diffusion coefficients were measured directly in these cells, or in GPMVs derived from these cells, containing cytosolic proteins only. Although the diffusion of the 3xeGFP and PEX5-eGFP became faster in the GPMVs as expected (50), the ratio of the two different diffusion proteins remained comparable (2.42 in cells and 1.96 in GPMVs). Each dot in the graph represents an individual FCS measurement, performed on three independent biological replicates. On the right, a microscopic image of the measured GPMVs containing eGFP-labeled proteins is shown. Scale bar, 10 μm. (*c*) The cytosolic diffusion of PEX5L is independent of PEX14. PEX5L was expressed together with eGFP-PTS1 in human fibroblasts (GM 5756T), HEK 293 cells, and the HEK KOPEX14 cell line. The diffusion coefficient of PEX5L was measured in WT fibroblasts (GM5657T), WT HEK cells (HEK 293), and WT HEK cells with without (knocked-out) PEX14 (HEK 293 PEX14 KO). The diffusion coefficients are comparable in all three cell lines, highlighting no influence by PEX14 on the diffusion of PEX5L. Each dot in the graph represents an individual FCS measurement. Bars represent the mean and standard deviation.

to as PEX5L N-Term and PEX5L C-Term), expressed them together with eGFP-PTS1 (in dual-expression plasmids) in human fibroblasts, and determined their diffusion coefficients as well as co-diffusion with eGFP-PTS1 using FCS and FCCS as already described. From theory, we would expect binding and, thus, co-diffusion and a non-zero cross-correlation curve for PEX5L C-Term and no binding and zero cross-correlation for PEX5L N-Term.

As expected, FCCS highlighted co-diffusion and, thus, binding between PEX5L C-Term and eGFP-PTS1, while PEX5L N-Term did not (Fig. 7 *b*). On the other hand, mobility of PEX5L N-Term was similarly slow ($D = 13 \pm 5.5$ $\mu m^2/s$) as full-length PEX5L ($D = 11.5 \pm 4.5$ $\mu m^2/s$) and PEX5L S600W ($D = 12 \pm 5$ $\mu m^2/s$), while diffusion of PEX5L C-Term was 2-fold faster ($D = 21.5 \pm 10$ $\mu m^2/s$) and about the same as 3xeGFP ($D = 22 \pm 5$ $\mu m^2/s$) (Fig. 7 *a*). Interestingly, PEX5L C-Term and PEX5L N-Term have similar MW (58 kDa and 56.5 kDa, respectively). Therefore, we concluded that the factors responsible for the slow diffusion of the cargo receptor PEX5 are molecular parts located in the protein's N-terminal half (e.g., their structurally large disorder) and/or other molecules interacting with this part.

The slow diffusion of PEX5L N-terminal half is caused by a cytosolic factor

The finding that the N-terminal half of PEX5L is responsible for the slow diffusion of the protein raised the question as to whether this slow diffusion was caused by cytosolic N-terminal binding partners or by the structurally disordered nature of the N-terminal half compared with the more ordered C-terminal PTS1 binding domain. Therefore, we compared the mobility of PEX5L N-Term with that of a similarly unstructured protein, the N-terminal half of PEX5 from *T. brucei*. While the structural architecture of PEX5L (and therefore also of its N-terminus) is similar between trypanosomes and the human PEX5L protein (Figs. 8 *a* and S3), we expected cytosolic interactions to differ between both variants due to their evolutionary distance. Therefore, we expressed the N-terminal half of human PEX5L (*Hs*PEX5L N-Term, aa 1–335) and the N-terminal half of PEX5 from *Trypanosoma* (*Tb*PEX5 N-Term, aa 1–340) in human fibroblast cells (labeled via SiRo-SNAP as before). Here, *Tb*PEX5 N-Term diffused almost twice as fast as its human counterpart ($D = 11 \pm 4$ $\mu m^2/s$ vs. 17 ± 6 $\mu m^2/s$) (Fig. 8 *c*). Consequently, the bulky unstructured character of the N-terminal part of PEX5 was not the main reason for the slowdown in diffusion.

To test whether this effect was thus rather caused by a cytosolic interaction partner of the human PEX5L, we created recombinant versions of the two proteins, both fused to eGFP. This allowed us to measure the diffusion of the proteins in solution, i.e., without the presence of any potential binding partner. Here, both *Hs*PEX5L N-Term and *Tb*PEX5 N-Term diffused equally fast ($D = 53 \pm 6$ $\mu m^2/s$ vs. 53 ± 6 $\mu m^2/s$) (Fig. 8 *d*).

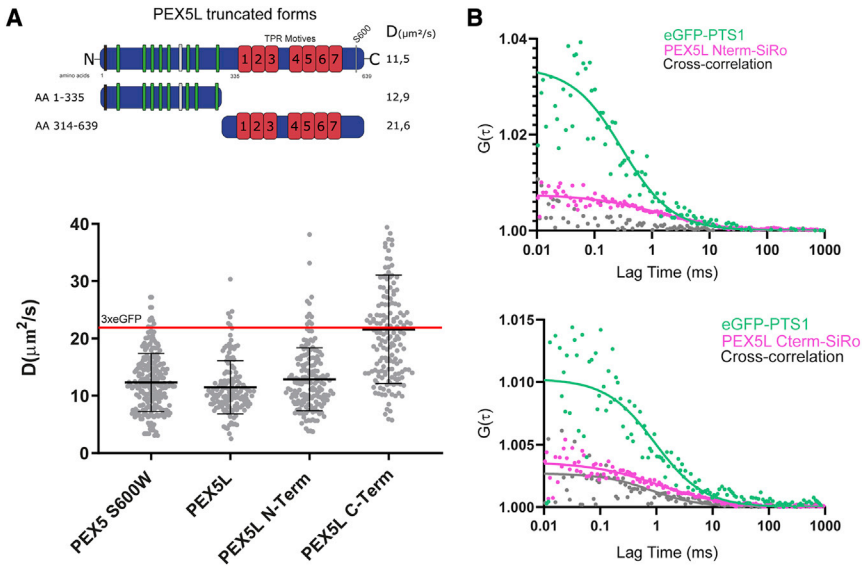

FIGURE 7 The N-terminal part of PEX5 slows down its diffusion. (*a*) Schematic representation of PEX5L. PEX5L can be divided into two different functional parts, the unstructured N-terminus (aa 1–335) with the WxxxxF/Y (green) motifs and the globular C-terminus (aa 314–639) with seven TPR motifs (red), which are interacting with the PTS1 proteins. The PEX7 binding site is shown in gray and the ubiquitin binding site in black at the very C-terminus. Truncated versions of the full-length PEX5L were created to analyze the diffusion of the two functional parts of PEX5L separately. PEX5L S600W (which cannot interact with PTS1 cargo proteins), PEX5L, PEX5L(1–335) (N-Term), and PEX5(314–639) (C-Term) were expressed separately in human fibroblasts and their diffusion coefficients were measured using FCS. The C-terminus diffused at 21.6 ± 9.4 $\mu m^2/s$ and the N-terminus at 12.9 ± 5.5 $\mu m^2/s$, similarly to the full-length PEX5L (11.5 ± 4.6 $\mu m^2/s$), indicating that this part defines the diffusion speed of the full-length protein. Each dot in the graph represents an individual FCS measurement (refer to "confocal live-cell FCS measurements" in materials and methods). Bars represent the mean and standard deviation. (*b*) The auto-correlation functions of eGFP-PTS1 (green) and PEX5L N-terminus (*upper*) or PEX5L-C-terminus (*lower*) (magenta) are displayed. The C-terminus of PEX5L diffused together with the eGFP-PTS1 cargo protein, as a cross-correlation could be measured, while the N-terminus of PEX5L did not diffuse together with the cargo protein. Here, no cross-correlation could be detected.

We then isolated cytosolic components from HEK 293 cells and incubated them with the recombinant proteins *Hs*PEX5L N-Term and *Tb*PEX5 N-Term (Fig. 8 *b*). Interestingly, the human-based cytosolic components specifically slowed human PEX5L N-Term (D = 7 ± 5 $\mu m^2/s$) but not its trypanosomal counterpart (D = 68 ± 6 $\mu m^2/s$); *Tb*PEX5 N-Term even diffused faster, which could for example be induced by cleavage actions from other factors such as human proteases (Fig. 8 *d*). Nevertheless, our data indicated that an interaction with a human-specific cytosolic binding partner was the most probable cause of slowdown in diffusion.

DISCUSSION

In this study, we applied advanced microscopy and spectroscopy techniques combined with biochemical methods to investigate the diffusion behavior of the peroxisomal import receptor PEX5 and its peroxisomal cargo proteins in the cellular cytosol. This combinatory approach established a toolbox necessary to reveal a broad range of biophysical information on cargo recognition and the migration behavior of the free and cargo-loaded receptor in the cytosol.

Using FCS, we were able to fully characterize the diffusion properties of PEX5 and reveal and characterize features expected from its function in peroxisomal protein import: 1) co-diffusion in a complex with cargo proteins, proved by the cross-correlation of PEX5 and PTS1 (Fig. 2 *b*); 2) diffusion of the major fraction of PTS1 in a complex with PEX5 (≈75%), and only a minor part with free diffusion characteristics, i.e., not bound to PEX5 (≈25%), but this distribution might be influenced by the overexpression of the proteins in this experimental setup; 3) by cross-correlation analysis employing C- and N-terminal truncations of PEX5, we demonstrated in living cells that the C-terminal part but not the N-terminal part of PEX5 binds PTS1 cargo proteins (Fig. 7 *b*), which formerly has only been seen in vitro (57); 4) using super-resolution AO z-STED-FCS, we proved cytosolic free diffusion of PEX5 (Fig. 4 *c*).

Strikingly, the analysis of the diffusion characteristics of PEX5 also revealed a very slow cytosolic diffusion of PEX5, which was much slower than expected from its MW. Furthermore, this slow diffusion was independent of 1) binding of PTS1-cargo (Fig. 2) and cargo type (Fig. 3 *a*), 2) interaction with PTS2 cargo and its cargo receptor PEX7 (Fig. 3 *b*), 3) possible (transient) interactions with peroxisomal membranes and other organelles (using PEX14 KO cells and GPMVs) (Fig. 6 *c*), 4) cytoskeleton meshwork (Fig. 6 *b*), 5) the structurally disordered N-terminal half of PEX5 (Figs. 7 and 8 *c*), and 6) possible and non-confirmed cytosolic oligomerization (Fig. 5).

Related to the last issue, PEX5 binding of oligomerized cargo proteins has been reported before, as it is a precondition of piggy-back transport of proteins into peroxisomes (58,59). Along this line, a dimeric alanine-glyoxylate aminotransferase could also bind two PEX5 receptors (22). However, it is still a matter of debate whether PEX5 binds oligomerized cargoes, which then can form large complexes with several receptor proteins involved. This "preimplex" hypothesis

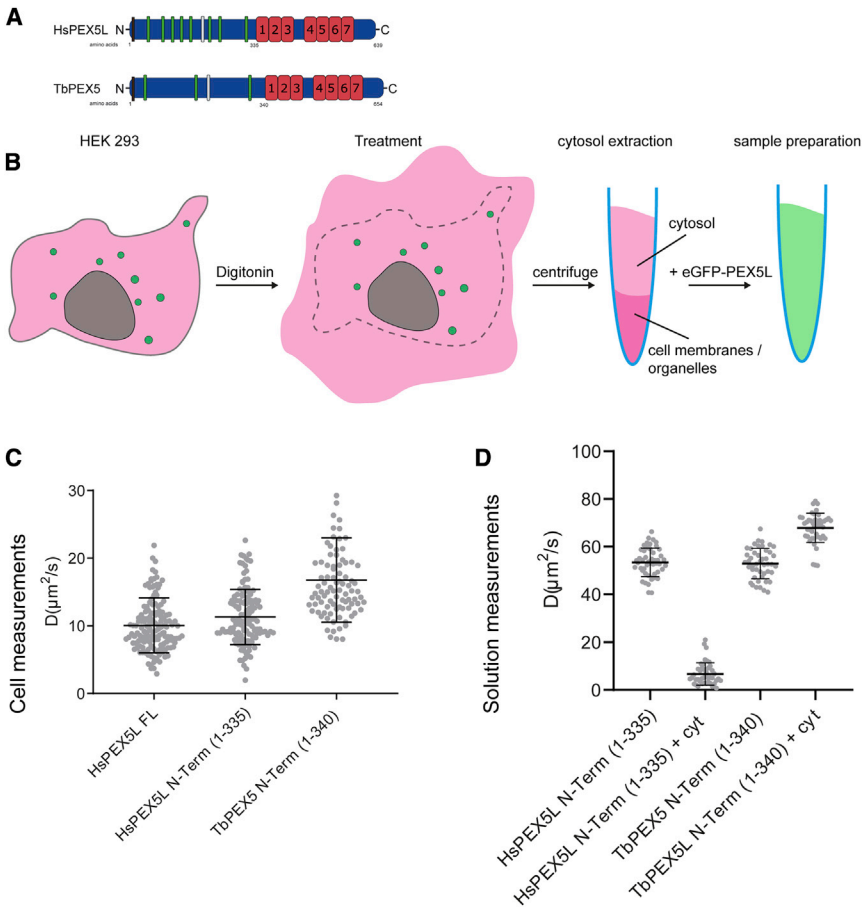

FIGURE 8 The slow diffusion of human PEX5 is caused by a cytosolic factor. (*a*) Architectural similarity of human and trypanosomal PEX5. The PTS1-receptor PEX5 from human and trypanosomes are similar in size and contain homologous structures, the C-terminal TPR motifs (red), which bind PTS1 cargo proteins, and the WxxxxF motifs in the N-terminal half (green), which mediate the binding of PEX5 to the peroxisomal membrane proteins PEX13 and PEX14. Also, both proteins contain a PEX7 binding site (gray) and a ubiquitin binding site (black) at the very N-terminus. (*b*) Extraction of the cytosol from human HEK 293 cells. Untreated HEK 293 cells were harvested and treated with a digitonin-containing buffer. The digitonin exclusively permeabilized the plasma membrane of the cells so that the cytosolic content was set free. After centrifugation, the cell membranes and organelles remained in the pellet while cytosolic proteins were found in the supernatant. This supernatant was mixed with the recombinant eGFP-labeled proteins and FCS was performed, resulting in values of *D*. (*c*) Diffusion coefficients in cells. Human fibroblasts were transfected with plasmids encoding for PEX5L, the N-terminal half of human PEX5L (*Hs*PEX5L N-Term, aa 1–335) and the N-terminal half of PEX5 from *Trypanosoma brucei* (*Tb*PEX5 N-Term, aa 1–340), and labeled with SNAP-SiRo. The diffusion coefficient of the human protein is significantly lower than the diffusion coefficient of the trypanosomal PEX5. Each dot in the graph represents an individual FCS measurement performed on three independent biological replicates. Bars represent the mean and standard deviation. (*d*) Diffusion coefficients in solution. *Hs*PEX5 N-Term-eGFP and *Tb*PEX5 N-Term-eGFP were recombinantly expressed in *E. coli* and purified. The diffusion coefficients of the human and trypanosomal N-terminal halves of PEX5 did not differ. The recombinant proteins were mixed with the cytosol isolated from human HEK cells. This led to a slowdown of the human PEX5L N-terminal half but not for the trypanosomal *Tb*PEX5 N-Term-eGFP. Each dot in the graph represents an individual FCS measurement (refer to "confocal live-cell FCS measurements" in materials and methods). Bars represent the mean and standard deviation.

was originally described by Gould and Collins (48) and is supported by findings that peroxisomal enzymes enter large protein complexes before they are translocated into the peroxisomal matrix (60). Although we cannot exclude possible very short and transient interactions, our data indicated no presence of PEX5 oligomerization in the cytosol, which is in line with other previous studies (53).

Finally, we compared cytosolic diffusion of human PEX5L with that of PEX5 from *T. brucei* (61), disclosing distinct mobility differences. From the fact that *Tb*PEX5 diffused faster than its human counterpart in the cytosol of mammalian cells, we discovered 1) that the unstructured N-terminus of PEX5 is not the cause for the non-typical slow diffusion of the receptor but that it only has a minimal influence on its mobility (as both variants are characterized by such an unstructured part), and 2) that the slow diffusion of PEX5 is not caused by the structure of the protein but by binding to another cytosolic protein. This was confirmed by in vitro measurements on recombinant human PEX5 and *Tb*PEX5. While both recombinant variants of PEX5 showed no difference in their diffusion behavior in solution, only the human PEX5 was slowed down in the presence of cytosolic proteins. In addition, diffusion of PEX5L was very distinctly slow rather than heterogeneous over a larger range of mobilities, i.e., the interaction was rather stable and non-transient. These findings point to a so far unknown cytosolic interaction partner that binds to the N-terminal part of human PEX5 and determines its peculiar diffusion behavior. The identity of this interaction partner still remains to be shown. Possible are interactions with a larger chaperone assembly, which would accompany PEX5 in its recognition of cargo proteins or protect the intrinsically disordered N-terminal region of PEX5 from aggregation. Also, an interaction of PEX5 with ribosomes could be envisioned, which would be in line with the observation that the mRNAs for the synthesis of peroxisomal proteins are found near peroxisomes (62). In any event, as the next step we plan to identify this binding

partner using, for example, chromatographic isolation approaches in conjunction with mass spectroscopy.

Besides novel insights into diffusion and interaction dynamics of peroxisomal proteins and especially the essential cargo carrier and import protein PEX5 in the cytosol of living cells, our study highlights the potential of using complementary experimental tools from advanced fluorescence microscopy and spectroscopy over model systems as biochemical and molecular biology approaches to decipher molecular interactions in the cytosol by studying their diffusion dynamics. Here, the combinatory approach revealed characteristics of the cytosolic migration behavior of peroxisomal proteins and their receptor interaction before peroxisomal targeting and import, and disclosed the cytosolic interaction of the peroxisomal import receptor PEX5 with a novel interaction partner.

SUPPORTING MATERIAL

Supporting material can be found online at https://doi.org/10.1016/j.bpr.2022.100055.

AUTHOR CONTRIBUTIONS

S.G., K.R., A.B., P.C., I.U., J.O., J.S., and P.H. performed the experiments. E.S., F.S., and D.W. helped in analyzing the FCS data. W.S., R.E., and C.E. provided input on the experimental design.

DECLARATION OF INTERESTS

The authors declare no competing interests.

ACKNOWLEDGMENTS

We thank the Wolfson Imaging Centre, Oxford for providing microscope facility support for data acquisition and analysis as well as the Microverse Imaging Center, Jena. We acknowledge funding by the Wolfson Foundation, MRC (grant no. MC_UU_12010/unit programs G0902418 and MC_UU_12025), the Wellcome Trust (grant no. 104924/14/Z/14, Strategic Award 091911 (Micron)), MRC/BBSRC/EPSRC (grant no. MR/K01577X/1, MRC grant no. MC_UU_12010/unit programs G0902418 and MC_UU_12025), the EPA Cephalosporin Fund, the John Fell Fund, and the Deutsche Forschungsgemeinschaft (research unit 1905 "Structure and function of the peroxisomal translocon"; grant no. 322325142 "Super-resolution optical microscopy studies of peroxisomal protein import in the yeast *Saccharomyces cerevisiae*", Germany's Excellence Strategy – EXC 2051 – Project-ID 390713860, project number 316213987 – SFB 1278). P. C. acknowledges a postdoctoral fellowship from the Basque Government (POS_2018_1_0066 and POS_2019_2_0022).

REFERENCES

1. Schliebs, W., and W.-H. Kunau. 2006. PTS_2 co-receptors: diverse proteins with common features. *Biochim. Biophys. Acta.* 1763:1605–1612.
2. Meinecke, M., C. Cizmowski, …, R. Erdmann. 2010. The peroxisomal importomer constitutes a large and highly dynamic pore. *Nat. Cell Biol.* 12:273–277.
3. Dodt, G., and S. J. Gould. 1996. Multiple PEX genes are required for proper subcellular distribution and stability of Pex5p, the PTS1 receptor: Evidence that PTS1 protein import is mediated by a cycling receptor. *J. Cell Biol.* 135:1763–1774.
4. Galiani, S., D. Waithe, …, C. Eggeling. 2016. Super-resolution Microscopy Reveals Compartmentalization of Peroxisomal Membrane Proteins. *J. Biol. Chem.* 291:16948–16962.
5. Reglinski, K., M. Keil, …, R. Erdmann. 2015. Peroxisomal Import Reduces the Proapoptotic Activity of Deubiquitinating Enzyme USP2. *PLoS One.* 10:e0140685.
6. Ghosh, D., and J. M. Berg. 2010. A proteome-wide perspective on peroxisome targeting signal 1(PTS1)-Pex5p affinities. *J. Am. Chem. Soc.* 132:3973–3979.
7. Blouin, C. M., Y. Hamon, …, C. Lamaze. 2016. Glycosylation-Dependent IFN-γR Partitioning in Lipid and Actin Nanodomains Is Critical for JAK Activation. *Cell.* 166:920–934.
8. Ladha, S., A. Mackie, …, H. Duclohier. 1996. Lateral diffusion in planar lipid bilayers: a fluorescence recovery after photobleaching investigation of its modulation by lipid composition, cholesterol, or alamethicin content and divalent cations. *Biophysical J.* 71:1364–1373.
9. Schwille, P., J. Korlach, and W. W. Webb. 1999. Fluorescence correlation spectroscopy with single-molecule sensitivity on cell and model membranes. *Cytometry.* 36:176–182.
10. Krichevsky, O., and G. Bonnet. 2002. Fluorescence correlation spectroscopy: the technique and its applications. *Rep. Prog. Phys.* 65:251–297.
11. Kim, S. A., K. G. Heinze, and P. Schwille. 2007. Fluorescence correlation spectroscopy in living cells. *Nat. Methods.* 4:963–973.
12. Elson, E. L. 2018. Introduction to fluorescence correlation Spectroscopy-Brief and simple. *Methods.* 140-141:3–9.
13. Schütz, G. J., H. Schindler, and T. Schmidt. 1997. Single-molecule microscopy on model membranes reveals anomalous diffusion. *Biophysical J.* 73:1073–1080.
14. Kusumi, A., C. Nakada, …, T. Fujiwara. 2005. Paradigm shift of the plasma membrane concept from the two-dimensional continuum fluid to the partitioned fluid: high-speed single-molecule tracking of membrane molecules. *Annu. Rev. Biophys. Biomol. Struct.* 34:351–378.
15. Manley, S., J. M. Gillette, …, J. Lippincott-Schwartz. 2008. High-density mapping of single-molecule trajectories with photoactivated localization microscopy. *Nat. Methods.* 5:155–157.
16. Eggeling, C., C. Ringemann, …, S. W. Hell. 2009. Direct observation of the nanoscale dynamics of membrane lipids in a living cell. *Nature.* 457:1159–1162.
17. Wachsmuth, M., W. Waldeck, and J. Langowski. 2000. Anomalous diffusion of fluorescent probes inside living cell nuclei investigated by spatially-resolved fluorescence correlation spectroscopy. *J. Mol. Biol.* 298:677–689.
18. Kues, T., R. Peters, and U. Kubitscheck. 2001. Visualization and tracking of single protein molecules in the cell nucleus. *Biophysical J.* 80:2954–2967.
19. Wachsmuth, M., T. Weidemann, …, J. Langowski. 2003. Analyzing intracellular binding and diffusion with continuous fluorescence photobleaching. *Biophysical J.* 84:3353–3363.
20. Fritzsche, M., and G. Charras. 2015. Dissecting protein reaction dynamics in living cells by fluorescence recovery after photobleaching. *Nat. Protoc.* 10:660–680.
21. Neuhaus, A., H. Kooshapur, …, R. Erdmann. 2014. A novel Pex14 protein-interacting site of human Pex5 is critical for matrix protein import into peroxisomes. *J. Biol. Chem.* 289:437–448.

22. Fodor, K., J. Wolf, …, M. Wilmanns. 2015. Ligand-induced compaction of the PEX5 receptor-binding cavity impacts protein import efficiency into peroxisomes. *Traffic.* 16:85–98.
23. Li, C., A. Wen, …, Y. Chang. 2011. FastCloning: a highly simplified, purification-free, sequence- and ligation-independent PCR cloning method. *BMC Biotechnol.* 11:92.
24. Shimozawa, N., Z. Zhang, …, N. Kondo. 1999. Functional Heterogeneity of C-Terminal Peroxisome Targeting Signal 1 in PEX5-Defective Patients. *Biochem. Biophysical Res. Commun.* 262:504–508.
25. De Walque, S., J. A. Kiel, …, P. A. Michels. 1999. Cloning and analysis of the PTS-1 receptor in Trypanosoma brucei. *Mol. Biochem. Parasitol.* 104:107–119.
26. Schliebs, W., J. Saidowsky, …, W. H. Kunau. 1999. Recombinant human peroxisomal targeting signal receptor PEX5 structural basis for interaction of PEX5 with PEX14. *J. Biol. Chem.* 274:5666–5673.
27. Holden, P., and W. A. Horton. 2009. Crude subcellular fractionation of cultured mammalian cell lines. *BMC Res. Notes.* 2:243.
28. Haeussler, M., K. Schonig, …, J. P. Concordet. 2016. Evaluation of off-target and on-target scoring algorithms and integration into the guide RNA selection tool CRISPOR. *Genome Biol.* 17:148.
29. Blayney, J., E. Foster, …, P. Hublitz. 2020. Unexpectedly High Levels of Inverted Re-Insertions Using Paired sgRNAs for Genomic Deletions. *Methods Protoc.* 3:53.
30. South, S. T., and S. J. Gould. 1999. Peroxisome Synthesis in the Absence of Preexisting Peroxisomes. *J. Cell Biol.* 144:255–266.
31. Clausen, M. P., E. Sezgin, …, C. Eggeling. 2015. A straightforward approach for gated STED-FCS to investigate lipid membrane dynamics. *Methods.* 88:67–75.
32. Waithe, D., M. P. Clausen, …, C. Eggeling. 2016. FoCuS-point: software for STED fluorescence correlation and time-gated single photon counting. *Bioinformatics.* 32:958–960.
33. Schneider, F., P. Hernandez-Varas, …, I. Urbancic. 2020. High photon count rates improve the quality of super-resolution fluorescence fluctuation spectroscopy. *J. Phys. D Appl. Phys.* 53:164003.
34. Schneider, F., T. Sych, …, E. Sezgin. 2021. Influence of nanobody binding on fluorescence emission, mobility, and organization of GFP-tagged proteins. *iScience.* 24:101891.
35. Steiert, F., E. P. Petrov, …, T. Weidemann. 2018. Photophysical Behavior of mNeonGreen, an Evolutionarily Distant Green Fluorescent Protein. *Biophysical J.* 114:2419–2431.
36. Barbotin, A., S. Galiani, …, M. J. Booth. 2019. Adaptive optics allows STED-FCS measurements in the cytoplasm of living cells. *Opt. Express.* 27:23378.
37. Weiss, M., M. Elsner, …, T. Nilsson. 2004. Anomalous Subdiffusion Is a Measure for Cytoplasmic Crowding in Living Cells. *Biophysical J.* 87:3518–3524.
38. Schwille, P., F. J. Meyer-Almes, and R. Rigler. 1997. Dual-color fluorescence cross-correlation spectroscopy for multicomponent diffusional analysis in solution. *Biophys. J.* 72:1878–1886.
39. Stanley, W. A., F. V. Filipp, …, M. Wilmanns. 2006. Recognition of a functional peroxisome type 1 target by the dynamic import receptor pex5p. *Mol. Cell.* 24:653–663.
40. Eggeling, C., J. Widengren, …, C. A. M. Seidel. 1998. Photobleaching of Fluorescent Dyes under Conditions Used for Single-Molecule Detection: Evidence of Two-Step Photolysis. *Anal. Chem.* 70:2651–2659.
41. Schneider, F., D. Waithe, …, M. Fritzsche. 2018. Statistical Analysis of Scanning Fluorescence Correlation Spectroscopy Data Differentiates Free from Hindered Diffusion. *ACS Nano.* 12:8540–8546.
42. Lenne, P.-F., L. Wawrezinieck, …, D. Marguet. 2006. Dynamic molecular confinement in the plasma membrane by microdomains and the cytoskeleton meshwork. *EMBO J.* 25:3245–3256.
43. Kastrup, L., H. Blom, …, S. W. Hell. 2005. Fluorescence Fluctuation Spectroscopy in Subdiffraction Focal Volumes. *Phys. Rev. Lett.* 94:178104.
44. Sezgin, E., F. Schneider, …, C. Eggeling. 2019. Measuring nanoscale diffusion dynamics in cellular membranes with super-resolution STED–FCS. *Nat. Protoc.* 14:1054–1083.
45. Ringemann, C., B. Harke, …, C. Eggeling. 2009. Exploring single-molecule dynamics with fluorescence nanoscopy. *New J. Phys.* 11:103054.
46. Gao, P., B. Prunsche, …, G. U. Nienhaus. 2017. Background suppression in fluorescence nanoscopy with stimulated emission double depletion. *Nat. Photon.* 11:163–169.
47. Lanzanò, L., L. Scipioni, …, G. Vicidomini. 2017. Measurement of nanoscale three-dimensional diffusion in the interior of living cells by STED-FCS. *Nat. Commun.* 8:65.
48. Gould, S. J., and C. S. Collins. 2002. Peroxisomal-protein import: is it really that complex? *Nat. Rev. Mol. Cell Biol.* 3:382–389.
49. Kong, J., Y. Ji, …, J. B. Kim. 2020. Spatiotemporal contact between peroxisomes and lipid droplets regulates fasting-induced lipolysis via PEX5. *Nat. Commun.* 11:578.
50. Schneider, F., D. Waithe, …, E. Sezgin. 2017. Diffusion of lipids and GPI-anchored proteins in actin-free plasma membrane vesicles measured by STED-FCS. *Mol. Biol. Cell.* 28:1507–1518.
51. Sezgin, E., H. J. Kaiser, …, I. Levental. 2012. Elucidating membrane structure and protein behavior using giant plasma membrane vesicles. *Nat. Protoc.* 7:1042–1051.
52. Will, G. K., M. Soukupova, …, R. Erdmann. 1999. Identification and characterization of the human orthologue of yeast Pex14p. *Mol. Cell. Biol.* 19:2265–2277.
53. Costa-Rodrigues, J., A. F. Carvalho, …, J. E. Azevedo. 2005. Pex5p, the Peroxisomal Cycling Receptor, Is a Monomeric Non-globular Protein. *J. Biol. Chem.* 280:24404–24411.
54. Shiozawa, K., P. V. Konarev, …, D. I. Svergun. 2009. Solution structure of human Pex5.Pex14.PTS1 protein complexes obtained by small angle X-ray scattering. *J. Biol. Chem.* 284:25334–25342.
55. Freitas, M., T. Francisco, …, J. E. Azevedo. 2011. PEX5 binds monomeric catalase blocking its tetramerization, and releases it upon binding the N-terminal domain of PEX14. *J. Biol. Chem.* 286:40509–40519.
56. Saidowsky, J., G. Dodt, …, W. Schliebs. 2001. The Di-aromatic pentapeptide repeats of the human peroxisome import receptor PEX5 are separate high-affinity binding sites for the peroxisomal membrane protein PEX14. *J. Biol. Chem.* 276:34524–34529.
57. Harano, T., S. Nose, …, Y. Fujiki. 2001. Hsp70 regulates the interaction between the peroxisome targeting signal type 1 (PTS1)-receptor Pex5p and PTS1. *Biochem. J.* 357:157.
58. McNew, J. A., and J. M. Goodman. 1994. An oligomeric protein is imported into peroxisomes in vivo. *J. Cell Biol.* 127:1245–1257.
59. Glover, J. R., D. W. Andrews, and R. A. Rachubinski. 1994. Saccharomyces cerevisiae peroxisomal thiolase is imported as a dimer. *Proc. Natl. Acad. Sci. U S A.* 91:10541–10545.
60. Bellion, E., and J. M. Goodman. 1987. Proton ionophores prevent assembly of a peroxisomal protein. *Cell.* 48:165–173.
61. Sampathkumar, P., C. Roach, …, W. G. Hol. 2008. Structural insights into the recognition of peroxisomal targeting signal 1 by trypanosoma brucei peroxin 5. *J. Mol. Biol.* 381:867–880.
62. Zipor, G., L. Haim-Vilmovsky, …, J. E. Gerst. 2009. Localization of mRNAs coding for peroxisomal proteins in the yeast, Saccharomyces cerevisiae. *Proc. Natl. Acad. Sci. U S A.* 106:19848.